Front. Mater. Sci. 2015, 9(1): 77–84
DOI 10.1007/s11706-015-0273-0

RESEARCH ARTICLE

Effect of chromium content on microstructure and corrosion behavior of W–Cr–C coatings prepared on tungsten substrate

Yan JIANG, Jun-Feng YANG, and Qian-Feng FANG (✉)

Key Laboratory of Materials Physics, Institute of Solid State Physics, Chinese Academy of Sciences, Hefei 230031, China

ABSTRACT: W–Cr–C coatings with different chromium contents (0–3 wt.%) were fabricated on the tungsten substrates by spark plasma sintering (SPS) method from the graphite and chromium mixed powders. SEM and XRD were exploited to analyze the effect of Cr contents on the microstructure of coatings. It was found that the abnormal hollow WC grains disappeared with addition of Cr less than 2%, and the microstructures were largely refined and densified. With further increase of Cr addition, the grains changed slightly but the densification was reduced. The most dense coating was achieved at 1 wt.% Cr. Corrosion behavior of the W–Cr–C coatings were investigated by impedance spectrum and potentiodynamic polarization tests. Results suggested that the W–1Cr–C coated W sample exhibited the lowest corrosion current density and highest corrosion potential due to the most densified microstructure, indicating that the addition of Cr at 1 wt.% was optimal for WC coating against corrosion.

KEYWORDS: W–Cr–C coating; spark plasma sintering (SPS); corrosion resistance; electrochemical measurement

Contents

Received October 20, 2014; accepted November 27, 2014

E-mail: qffang@issp.ac.cn

1 Introduction

Owing to good thermal conductivity, high hardness and high melting point, tungsten has been considered as one of the candidate materials applied in nuclear fusion and spallation neutron source environments [1–2]. Especially, when acting as the spallation target the tungsten faced serious erosion-corrosion in heavy water, and this corrosion could be exacerbated by the presence of neutron irradiation [3–4]. To make this problem less serious, two promising measures were taken into consideration. One is to alternate the target with improved metal or alloy materials, and the other is to clad the pure tungsten with more corrosion-resistant materials. The first approach was found to bring about a severe reduction of the neutron yield [5], whereas the latter approach can retain both the

spallation yield and the thermal advantage of tungsten.

By contrast, fabrication of corrosion-resistant coating on pure tungsten would be the more practicable option to protect tungsten from corrosion. To our knowledge, tungsten carbide (WC) coating was reported as a chemically stable material, which had favorable properties in wear, oxidation and corrosion resistance [6], and was widely used as favorable protector of metallic matrix in engineering and manufacturing field than other conventional carbide coatings. Other than that, WC exhibits a good capacity of heat conduction with thermal conductivity being 84 $W \cdot m^{-1} \cdot K^{-1}$ [7]. However, it is difficult to fabricate dense pure WC, so binder agents, for example Co, are normally introduced to enhance the consolidation of WC at a relatively lower temperature, owing to the low melting point of Co (1768 K) and good wettability of Co to WC [8–10]. Although the wear resistance and fracture toughness of tungsten carbide were improved by introducing Co [11–12], the corrosion resistance of WC–Co was reduced in liquid environment owing to the poor corrosion resistance of Co [10,13–15]. Therefore, a substitution of Co by other agent, that could enhance the densification of WC meanwhile not reduce the corrosion resistance in the liquid environment, has to be taken into consideration.

Chromium carbide was reported to exhibit excellent strength, hardness, corrosion and wear resistance [16]. When it was integrated into the surface of metallic alloys, it can develop the wear and corrosion resistance of the alloys, and maintain these properties at elevated temperatures. So, chromium carbide was often served as a useful additive in the surface treatment of alloys [17–18]. Besides, it was also believed that addition of certain content of chromium carbide could improve the densification of refractory cermet during high-temperature sintering [19]. In one of our previous work [20], it was found that the W–6wt.%Cr–C coating consisting of nanocrystalline WC and Cr–C nodules exhibited a better corrosion resistance than pure WC coating. However, the addition of 6 wt.% Cr caused the formation of big Cr-rich protruding nodules with some micro cracks owing to the little inter-solubility between chromium carbide and tungsten carbide in the case of binder-less sintering, therefore the content of Cr in the W–Cr–C coatings should be optimized to obtain W–Cr–C coatings with high performance. In this work, the W–Cr–C coatings with lower Cr content in the range of 0.5%–3% were fabricated, and the effect of Cr content on the microstructure and corrosion behavior of W–Cr–C coatings were investigated in details.

2 Experimental

The substrate materials were commercial tungsten (99.9%) with dimensions of about 2 mm in thickness and 15 mm in diameter. The substrates were polished by different abrasive papers (P400, P800, P1500, P2000 and W2.5, sequentially) and degreased by acetone. Four different contents of Cr powders (0.5, 1, 2 and 3 wt.%) mixed with graphite were used as the source of carbon and chromium. The four varieties of W–Cr–C coatings were fabricated on smooth W substrates by spark plasma sintering (SPS) method from the mixed powders. The sintering program was the same as in Ref. [20]. For comparison, the pure WC-coated W samples were also prepared using the same program by covering with graphite powder on tungsten substrate. After sintering, the coating surface were slightly polished with a polishing cloth to remove the contaminant, and then rinsed in acetone for the next measurements. The effect of Cr content on the microstructure of WC coating was observed by field-emission scanning electron microscopy (FESEM, Sirion200, FEI) and energy-dispersive X-ray spectroscopy (EDS).

Corrosion behavior was evaluated by electrochemical experiments. Measurement was performed on an electrochemical station (Parstat 4000) coupled with a three-electrode cell. Saturated calomel electrode (SCE) and platinum plate were used as the reference and counter electrode, respectively. A working area of 0.667 cm^2 was exposed to the 3.5 wt.% NaCl electrolyte solution. After potential stabilization of the system, the electrochemical impedance spectroscopy (EIS) test was carried out with the amplitude of 10 mV and frequencies ranging from 10^5 to 0.1 Hz. The potentiodynamic polarization curves were swept from −250 mV (*vs.* open circuit) to 0.45 V at a scanning rate of 0.167 $mV \cdot s^{-1}$. The results were analyzed with Zsimpwin software.

3 Results and discussion

3.1 XRD pattern

Figure 1 displays the X-ray diffraction (XRD) patterns of W–Cr–C coatings with different Cr content. The WC phase can be clearly detected in all samples with Cr addition from 0.5% to 3%. In the coatings containing Cr over 2%, orthorhombic Cr_3C_2 phase is detected, and its diffraction peak corresponding to (320) plane is indicated in Fig. 1. In the coatings containing less Cr, however, such chromium

carbide phase is difficult to be detected by XRD owing to the low content. Combined with the results in Ref. [20], it can be concluded that the coatings fabricated on pure W substrates were composed of WC and different contents of chromium carbides, and the chromium carbides were gathered into nodules concentrating in the surface layer of W–Cr–C coatings. As the distribution of chromium carbide particles were scattered on surface, the following work was just to investigate the surface microstructure of WC grains and its variation with Cr content.

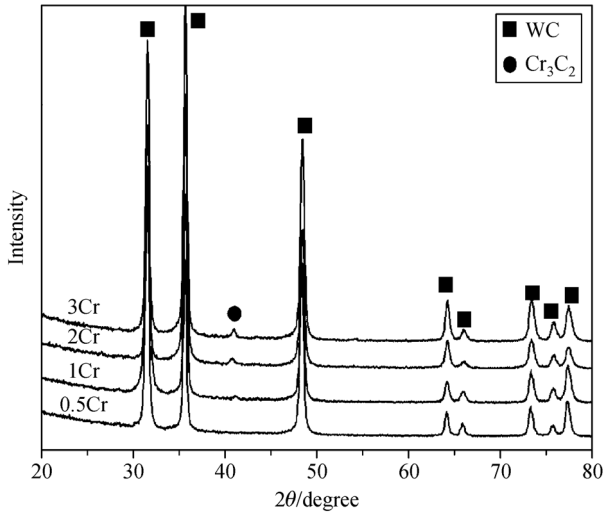

Fig. 1 XRD patterns of W–Cr–C coatings with the Cr addition from 0.5% to 3%.

3.2 Microstructure

Figures 2(a)–2(f) show the surface microstructures of W–Cr–C coatings with Cr content from 0 to 3 wt.%. The corresponding size distribution of WC grains was displayed in Fig. 3, which was conducted by counting about 400 grains in the scanning electron microscopy (SEM) images. It was observed that the surface morphology of WC coatings was largely modified by the Cr addition. In the case without Cr addition, the pure WC coating (Fig. 2 (a)) was composed of wide grain boundaries and abnormally grown grains that looked like inhomogeneously distributed hollow bars with length on the order of 2–5 μm. As 0.5 wt.% Cr was incorporated, the abnormal WC grains almost disappeared, instead, the WC grains were grown up to solid granular and compact structure (Fig. 2 (b)), and became refined. The size distribution of WC grains in W–0.5Cr–C coating is in the range between 500 nm to 2 μm with an average grain size of about 1.3 μm, as depicted in Fig. 3. When Cr content increases to 1 wt.% (Fig. 2(c)), the microstructure of W–Cr–C coating was more refined and compact, without obvious variation of grain shape. The size distribution of WC grains in W–1Cr–C coating becomes narrower and the average grain size is about 0.9 μm. With further increase of Cr, the abnormal hollow WC grains appeared again that led to presence of micro porosity (Figs. 2(d) and 2(e)). Meanwhile, some plate-like WC grains appeared on the surface of W–3Cr–C coating (Fig. 2(f)). The plates had no regular arrangement due to the special fabrication method in this work which differed from the conventional sintering of bulk alloy. The grain size distribution of W–2Cr–C and W–3Cr–C coatings is similar and the average grain size is about 0.7 μm (Fig. 3).

From the variations in morphology of W–Cr–C coatings, it can be concluded that Cr addition could induce both prominent densification and refinement effects, especially at contents of 1 wt.% Cr. The densification effect could be understood by the change of coating microstructure from hollow bar to solid granular type that narrowed the width of grain boundary and reduced the porosity of grain itself. However, the reason of WC grain refinement may be aroused in terms of several aspects. During the SPS process, there were two principal solid-phase reactions occurred between the interface of substrate and mixed powders, as shown in the schematic diagram of Fig. 4. One was the carbonization of chromium to form chromium carbide [20], the other was the inter-diffusion of carbon and tungsten to form gradient coatings of tungsten carbides [21]. As the former reaction occurred more readily due to the direct contact between C and Cr powders, so the chromium carbide formed prior to the WC and segregated in the surface layer of WC coating. Chromium carbide was known as an effective grain growth inhibitor in the fabrication of ultrafine-grained WC-based alloys. In the case of Co existence, three grain refinement mechanisms were suggested [19,22]: (i) adhesion of chromium carbide on WC grains reduced the solubility of WC in liquid Co; (ii) dissolution of chromium carbide in liquid Co lowered the solubility of WC grains [23]; (iii) segregation of chromium carbide blocked the migration of WC/WC interface. As for the binder-less sintering of W–Cr–C coatings in the present study, the refinement effect can be principally attributed to the third reason. In the case of the absence of binder phase (e.g. Co), the chromium carbide had a very low inter-solubility with WC, and the small chromium carbide grains formed on the surface layer

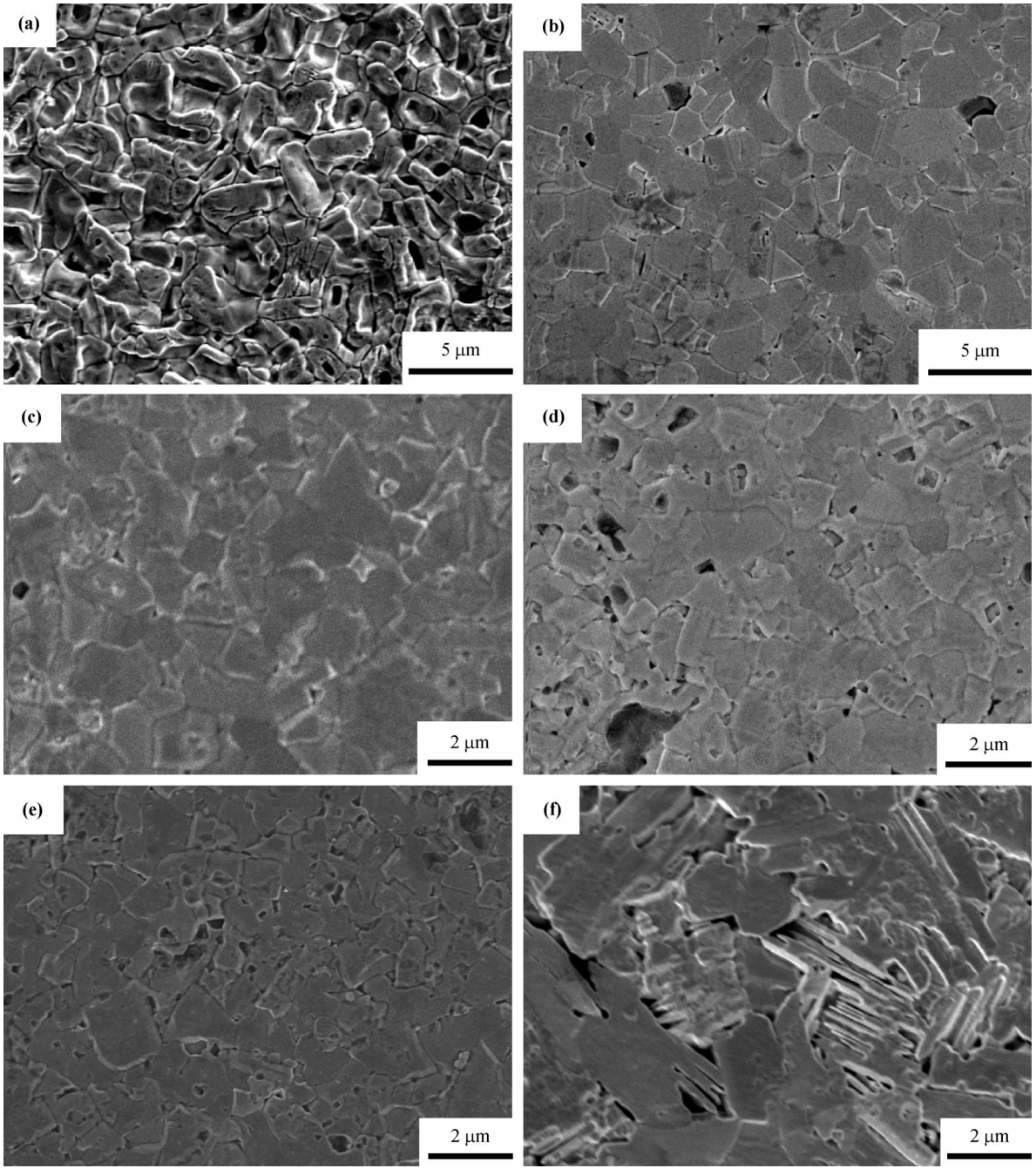

Fig. 2 Surface images of **(a)** pure WC coating, **(b)** W–0.5%Cr–C coating, **(c)** W–1%Cr–C coating, **(d)** W–2%Cr–C coating, **(e)** W–3%Cr–C coating, and **(f)** the plates on the surface of W–3%Cr–C coating.

would hinder the growth of WC grains. However, this refinement of WC grains would be saturated at higher Cr content because of the aggregation of chromium carbides caused by the increased area fraction of chromium carbides. This maybe accounts for the fact that the grain size of WC phase changed slowly with further increasing of Cr content.

3.3 Corrosion resistance

The potentiodynamic polarization curves for the W–Cr–C coated samples with different Cr contents were shown in Fig. 5. The corresponding parameters such as corrosion potential (E_{corr}), corrosion current density (I_{corr}) and passivation current density were deduced from Fig. 5 and

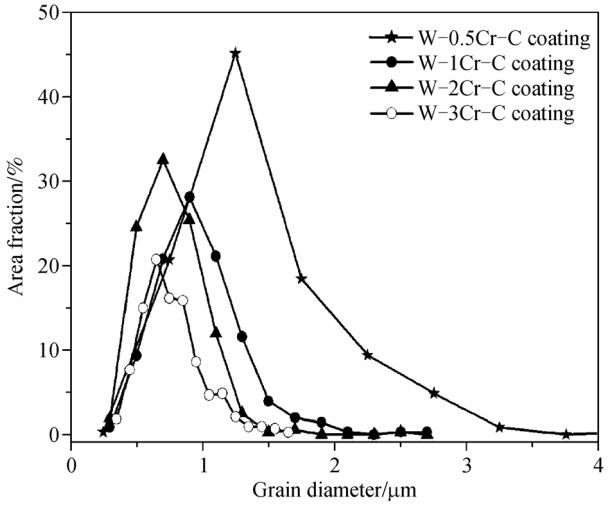

Fig. 3 Grain size distribution of the W–Cr–C coatings.

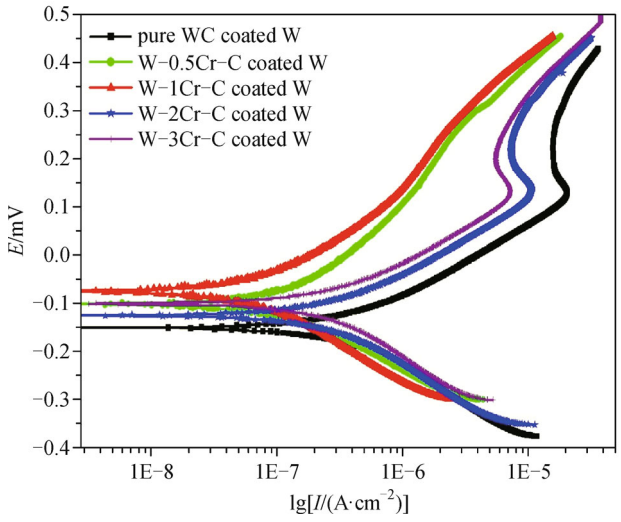

Fig. 5 Polarization curves for W–Cr–C coatings.

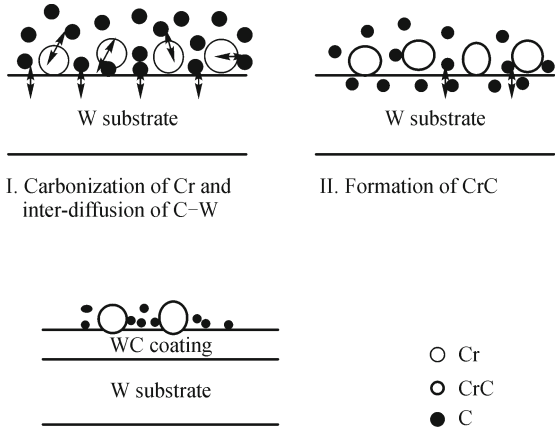

Fig. 4 Schematic diagram of solid-state reactions in the SPS process.

summarized in Table 1 [20]. According to the general shape of curves, two types of polarization behavior among the five coatings can be identified. One type is related to the W–0.5Cr–C and W–1Cr–C coatings, which displays a feature of active-dissolution behavior in the NaCl solution. As shown in Fig. 5, the current density of both W–0.5Cr–C and W–1Cr–C coatings increase with increasing anodic over voltage, and only a single active region is presented through the entire range of anodic polarization. In addition, it can be seen from Table 1 that the W–1Cr–C coating exhibits a lower I_{corr} (81 nA/cm^2) and a higher E_{corr} (-77 mV) than the W–0.5Cr–C coating, whose I_{corr} and E_{corr} are 165 nA/cm^2 and -102 mV, respectively.

The other type of polarization is related to the WC, W–2Cr–C and W–3Cr–C coatings, whose curves display a typical corrosion behavior containing four regions, i.e. active, active to passive transition, passive and transpassive regions. In the active region, the coatings experienced continuous corrosion process. The largest I_{corr} and lowest E_{corr} obtained for the pure WC coating confirmed that it suffered more corrosion than the Cr-contained coatings. With gradual formation of adhesive films on the coating surface, the current density of the specimens started to decrease from the maximum value, which is called passivation current density and stands for the transition of materials from active corrosion to passivation. The smaller the passivation current density is, the more beneficial it is for the passivation. As seen from Fig. 5 and Table 1, the values of passivation current density for the three coatings are sequenced as: W–3Cr–C < W–2Cr–C < WC, which means the W–Cr–C coatings have a faster formation speed of passivation than pure WC coating. However, unfavorably, the passive state was very temporary. After a quite narrow voltage range for passivation, the coatings began to enter into the transpassive stage, the current increased again and the samples corroded as before due to the instability of the passive film.

The distinct types of polarization behavior revealed a great influence of Cr amount on the corrosion behavior of WC coatings. Pure WC coating showed a passive feature in the sodium chloride solution with a short passive range of about 100 mV. After incorporation of small amount of Cr (no more than 1%), the passive behavior disappeared and replaced by an active-dissolution behavior with lower corrosion rate. As the Cr addition increased over 1%, the passivation appeared again. These variations of corrosion behavior can be attributed to the microstructures of the

Table 1 Corrosion data for the W–Cr–C coatings in the active region

Coating composition	E_{corr} /mV	I_{corr} /(nA·cm^{-2})	Passivation current density /(μA·cm^{-2})
WC–0Cr	–151 [20]	400 [20]	13.5
WC–0.5%Cr	–102	165	–
WC–1%Cr	–77	81	–
WC–2%Cr	–126	292	7
WC–3%Cr	–107	283	4.8

coatings that have been changed through the different Cr addition. According to our knowledge, corrosion occurred mainly on the defect locations of surface, so the intergranular corrosion or pitting corrosion was often much severer than the corrosion of the grain. In this study, the compact granular structures of W–0.5Cr–C and W–1Cr–C coatings strongly reduced the grain-boundary width and the pitting-corrosion degree induced by the abnormal growth of WC grains, resulting in a large decrease of the corrosion current. It is worth noting that the more compact W–1Cr–C coating showed a smaller corrosion current than the W–0.5Cr–C coating. Besides, the decreased pitting sites and grain-boundary width reduced the number of adhesion locations for corrosion products, which resulted in the failure of passive film's formation and the electrochemical polarization in electrode reactions. Eventually, the coatings presented a continuous active dissolution in the entire range of anodic polarization. This may be the reason why the polarization behaviors of W–0.5Cr–C and W–1Cr–C coatings were different from the others.

On the other hand, the lower passivation current density for W–2Cr–C and W–3Cr–C coatings was related to the refinement of the microstructure. Microstructural refinement produced higher grain boundary density, which provided larger fraction of nucleation sites for passivation, showing a faster formation speed of passive film than pure WC coating with coarse grains.

In spite of the passive behaviors of W–2Cr–C and W–3Cr–C coatings, the passivity was so unsteady that it was hard to build a barrier layer applicable for anodic protection against corrosion. Generally speaking, the W–1Cr–C coating with minimum corrosion current was more corrosion resistant than other Cr-contained coatings fabricated in this work.

The Nyquist and Bode-phase spectra measured for the W–Cr–C coatings were shown in Fig. 6. The complex-impedance spectroscopy of all coatings displayed a semicircular shape in the low frequency region, which indicates that the response of Warburg impedance caused by diffusion process has not occurred yet. Combined with

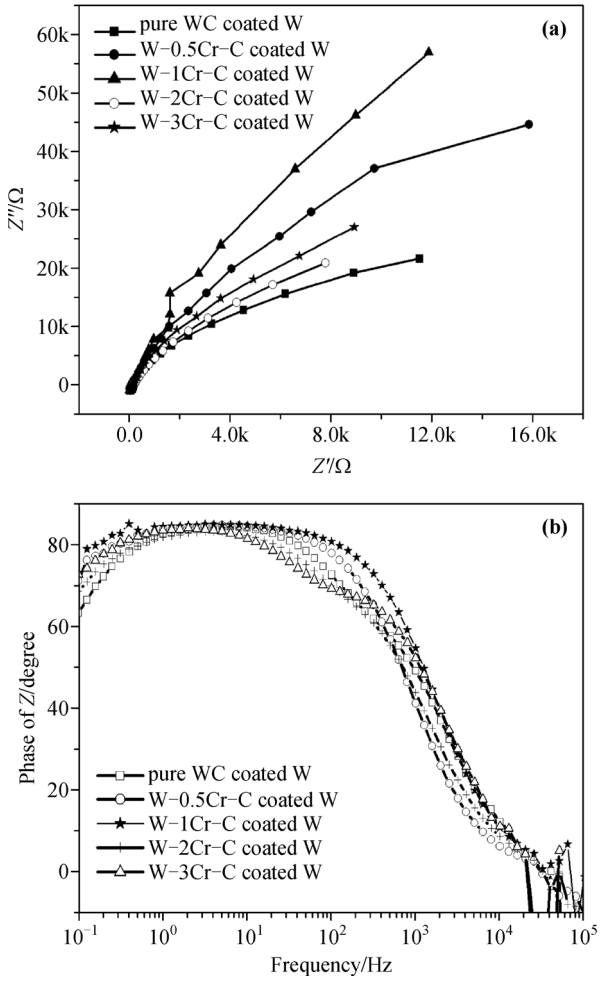

Fig. 6 **(a)** Nyquist and **(b)** Bode-phase spectra for the W–Cr–C coatings.

the variation feature of the phase angle, it can be further concluded that all of the impedance spectra present bare response of capacitance arc, and the anodic reactions of all samples are under the control of charge transfer. Thereamong, the W–0.5Cr–C and W–1Cr–C coated samples show a single depressed overlapping capacitive semicircle, which follow a typical response model of one-time constant: $R_s(Q_{ct}R_{ct})$. In this model, a solution resistance (R_s) is in series with a parallel combination of a constant-

Table 2 Fitting data from EIS for the W–Cr–C coatings

Coating composition	R_S /($\Omega\cdot cm^2$)	CPE_p /($10^{-5}\,\Omega^{-1}\cdot cm^{-2}\cdot s^{-n}$)	n_p	R_p /($\Omega\cdot cm^2$)	CPE_{ct} /($10^{-5}\,\Omega^{-1}\cdot cm^{-2}\cdot s^{-n}$)	n_{ct}	R_{ct} /($10^4\,\Omega\cdot cm^2$)
WC–0Cr	3.1	9.76	0.99	3.9	5.3	0.94	4.37
WC–0.5%Cr	6.2	–	–	–	4.6	0.94	15.42
WC–1%Cr	4.3	–	–	–	3.9	0.94	37.94
WC–2%Cr	4.1	16.9	0.96	5.3	8.5	0.93	5.91
WC–3%Cr	3.6	9.4	0.98	12.3	7.4	0.94	8.60

phase element (Q) and a charge-transfer resistance (R_{ct}) of the compact layer of coating. Q used here, in place of a double-layer capacitor between solid electrode and solution, is to compensate for the dispersion effect resulting from the non-homogeneity of sample surface [24–25]. R_{ct} is proportional to the arc diameter and inversely proportional to the corrosion current density [26], the larger the diameter of the arc, the lower the current density and corrosion rate [27–28].

The equivalent circuit suitable for the W–2Cr–C, W–3Cr–C and pure WC-coated samples is a two-time constant model ($R_s(Q_pR_p)(Q_{ct}R_{ct})$), where Q_p and R_p are related to the constant phase element and resistance of porous outer layer of coating, respectively. The parameters of the two kinds of equivalent circuits were obtained by fitting the curves in Fig. 6 with the two models and listed in Table 2. Comparing the parameters shown in Table 2, it was observed that the W–1Cr–C coated sample exhibited the largest value of R_{ct} ($37.9\times10^4\,\Omega\cdot cm^2$), followed by the W–0.5Cr–C coating ($15.4\times10^4\,\Omega\cdot cm^2$). For the W–2Cr–C and W–3Cr–C coatings, although both R_{ct} and R_p are larger than that of the pure WC coating, they are still smaller than that of the lower Cr-added coatings. Thus, addition of 1 wt.% Cr at was the most appropriate for the improvement of corrosion resistance, which was in good agreement with the analysis results of the polarization test.

4 Conclusions

W–Cr–C composite coatings with addition of 0.5–3 wt.% Cr were successfully fabricated on W substrate by SPS method at the temperature of 1600ºC with duration of 10 min. Effects of different contents of Cr addition on the microstructure and corrosion resistance of WC coating were investigated. The grain size and morphology of WC coatings were remarkably changed with increasing Cr content until the addition was over 1 wt.%. The most compact microstructure was achieved for the W–1Cr–C coating. The polarization and Nyquist test in 3.5% NaCl solution also revealed that the W–1Cr–C coating has the lowest corrosion current density in protecting pure W substrate. From the above investigations concerning the impact of different contents of Cr addition on the electrochemical behavior, it was suggested that, among the three variables of densification, grain size and chromium carbide content, the densification play the most important role on the corrosion resistance of W–Cr–C coatings.

Abbreviations

EDS	energy-dispersive X-ray spectroscopy
EIS	electrochemical impedance spectroscopy
FESEM	field-emission scanning electron microscopy
SCE	saturated calomel electrode
SEM	scanning electron microscopy
SPS	spark plasma sintering
WC	tungsten carbide
XRD	X-ray diffraction

Acknowledgements This work was financially supported by the National Natural Science Foundation of China (Grant Nos. 11075177 and 51101152) and the Tribology Science Fund of State Key Laboratory of Tribology (Grant No. SKLTKF12B13).

References

[1] Guo S Q, Ge C C, Zhou Z J, et al. Research development of tungsten coatings used as plasma facing materials for fusion reactor. Materials Review, 2010, 24(3): 93–96 (in Chinese)

[2] Sommer W F, Maloy S A, Louthan M R, et al. Performance of a clad tungsten rod spallation neutron source target. Nuclear Technology, 2005, 151(3): 303–313

[3] Daemen L L, Kanner G S, Lillard R S, et al. Modeling of water radiolysis at spallation neutron sources. Conference: 126, Annual Meeting of the Minerals, Metals and Materials Society, Orlando, FL, USA, 1998, 83–91

[4] Noriaki N J, Keisuke K, Noboru A, et al. Corrosion resistance of tungsten and tungsten alloys for spallation target in stagnant and flowing water. Journal of the Japan Institute of Metals, 2002, 66:

1107–1115

[5] Nelson A T, O'Toole J A, Valicenti R A, et al. Fabrication of a tantalum-clad tungsten target for LANSCE. Journal of Nuclear Materials, 2012, 431(1–3): 172–184

[6] Yu L G, Khor K A, Li H, et al. Restoring WC in plasma sprayed WC–Co coatings through spark plasma sintering (SPS). Surface and Coatings Technology, 2004, 182(2–3): 308–317

[7] Shackelford J F, Alexander W. CRC Materials Science and Engineering Handbook. 3rd ed. Boca Raton: CRC Press LLC, 2001, 430

[8] Park H K, Youn H J, Lee S M, et al. Consolidation of ultra fine WC–Co hard materials by a spark plasma sintering method and their mechanical properties. Journal of Ceramic Processing Research, 2011, 12: 304–309

[9] Machado I F, Girardini I, Lonardelli I, et al. The study of ternary carbides formation during SPS consolidation process in the WC–Co–steel system. International Journal of Refractory Metals & Hard Materials, 2009, 27(5): 883–891

[10] Wentzel E J, Allen C. The erosion-corrosion resistance of tungsten carbide hard metals. International Journal of Refractory Metals & Hard Materials, 1997, 15(1–3): 81–87

[11] Saito H, Iwabuchi A, Shimizu T. Effects of Co content and WC grain size on wear of WC cemented carbides. Wear, 2006, 261(2): 126–132

[12] Bouaouadja N, Hamidouche M, Osmani H, et al. Fracture toughness of WC–Co cemented carbides at room temperature. Journal of Materials Science Letters, 1994, 13(1): 17–19

[13] Sutthiruangwong S, Mori G. Corrosion properties of Co-based cemented carbides in acidic solutions. International Journal of Refractory Metals & Hard Materials, 2003, 21(3–4): 135–145

[14] Kellner F J J, Hildebrand H, Virtanen S. Effect of WC grain size on the corrosion behavior of WC–Co based hardmetals in alkaline solutions. International Journal of Refractory Metals & Hard Materials, 2009, 27(4): 806–812

[15] Qiao Z H, Räthel J, Berger L M, et al. Investigation of binderless WC–TiC–Cr_3C_2 hard materials prepared by spark plasma sintering (SPS). International Journal of Refractory Metals & Hard Materials, 2013, 38: 7–14

[16] Singh V, Diaz R, Balani K, et al. Chromium carbide-CNT nanocomposites with enhanced mechanical properties. Acta Materialia, 2009, 57(2): 335–344

[17] Wu Q L, Li W G. The microstructure and wear properties of laser-clad WC–Cr_3C_2 cermet coating on steel substrate. Materials Transactions, 2011, 52(3): 560–563

[18] Xue M P, Han B, Wang Y, et al. Microstructure and corrosion resistance properties of Ni based WC/Cr_3C_2 coating prepared by laser cladding. Laser & Optoelectronics Progress, 2011, 48(9): 82–87 (in Chinese)

[19] Sun L, Jia C C, Cao R J, et al. Effect of Cr_3C_2 additions on the densification, grain growth and properties of ultrafine WC–11Co composites by spark plasma sintering. International Journal of Refractory Metals & Hard Materials, 2008, 26(4): 357–361

[20] Jiang Y, Yang J F, Xie Z M, et al. Corrosion resistance of W–Cr–C coatings fabricated by spark plasma sintering method. Surface and Coatings Technology, 2014, 254: 202–206

[21] Jiang Y, Yang J F, Zhuang Z, et al. Characterization and properties of tungsten carbide coatings fabricated by SPS technique. Journal of Nuclear Materials, 2013, 433(1–3): 449–454

[22] Wu E X, Lei Y W. Effect of inhibitor on ultrafine grained cemented carbides. Cemented Carbides, 2002, 19(3): 136–139

[23] Li N, Qiu Y X, Zhang W, et al. Influence and function of inhibitor VC/Cr3C2 on the grain growth in super fine WC–Co cermets. Rare Metal Materials and Engineering, 2007, 36(10): 1763–1766 (in Chinese)

[24] Cao C N, Zhang J Q. An Introduction to Electrochemical Impedance Spectroscopy. Beijing: Science Press, 2002 (in Chinese)

[25] Ahn S H, Yoo J H, Choi Y S, et al. Corrosion behavior of PVD-grown WC–($Ti_{1-x}Al_x$)N films in a 3.5% NaCl solution. Surface and Coatings Technology, 2003, 162(2–3): 212–221

[26] Aw P K, Tan A L K, Tan T P, et al. Corrosion resistance of tungsten carbide based cermet coatings deposited by high velocity oxy-fuel spray process. Thin Solid Films, 2008, 516(16): 5710–5715

[27] Zhu Q Z, Xue W B, Lu L, et al. Preparation of microarc oxidation coating on $(Al_2O_3–SiO_2)_{sf}$/AZ91D magnesium matrix composite and its electrochemical impedance spectroscopic analysis. Acta Metallurgica Sinica, 2011, 47(1): 74–80 (in Chinese)

[28] Manohar A K, Bretschger O, Nealson K H, et al. The use of electrochemical impedance spectroscopy (EIS) in the evaluation of the electrochemical properties of a microbial fuel cell. Bioelectrochemistry, 2008, 72(2): 149–154